Journal of Alloys and Compounds 509 (2011) 5050–5054

Contents lists available at ScienceDirect

Journal of Alloys and Compounds

journal homepage: www.elsevier.com/locate/jallcom

Changes of optical, dielectric, and structural properties of $Si_{15}Sb_{85}$ phase change memory thin films under different initializing laser power

Huan Huang [a], Lei Zhang [b], Yang Wang [a,*], Xiao Dong Han [b], Yiqun Wu [a], Ze Zhang [b,c], Fuxi Gan [a]

[a] Key Laboratory of High Power Laser Materials, Shanghai Institute of Optics and Fine Mechanics, Chinese Academy of Sciences, Shanghai 201800, China
[b] Institute of Microstructure and Property of Advanced Materials, Beijing University of Technology, Beijing 100124, China
[c] Department of Materials, Zhejiang University, Hangzhou, Zhejiang Province 310008, China

ARTICLE INFO

Article history:
Received 5 November 2010
Received in revised form 17 January 2011
Accepted 5 February 2011
Available online 12 February 2011

Keywords:
SiSb phase change film
Optical constant
Dielectric function
TEM

ABSTRACT

The optical, dielectric, and structural characteristics of $Si_{15}Sb_{85}$ phase change memory thin films under a moving continuous-wave laser initialization are studied by using spectroscopic ellipsometry and high-resolution transmission electron microscopy. The dependence of complex refractive index, dielectric functions, absorption coefficient, and optical band gap of the films on its crystallization extents formed by the different initialization laser power are analyzed in detail. The structural change from as-deposited amorphous phase to distorted rhombohedra-Sb-like crystalline structure with the increase of initialization laser power is clearly observed with sub-nanometer resolution. The optical and dielectric constants, the relationship between them, and the local atomic arrangements of this new phase change material can help explain the phase change mechanism and design the practical phase change memory devices.
© 2011 Elsevier B.V. All rights reserved.

1. Introduction

Since the demonstration of threshold switching by Ovshinsky [1], phase change materials have been investigated extensively for data storage applications. Phase change materials have been characterized by the unconventional combination of two main properties [2] namely, the pronounced change of optical and electrical properties on crystallization/amorphization and the crystallization/amorphization within a very short timescale. In recent decades, the property combination has resulted in the preference for chalcogenides for applications in reversible phase change optical discs and nonvolatile random access memory [3–7].

Te-based chalcogenide phase change materials, such as GeSbTe pseudo-binary alloys [7,8], have displayed outstanding performance in data storage applications. However, some problems remain [9]. The search for new materials with better performance has remained a necessary and challenging task. Recently, Zhang et al. [9–11] have reported that Te-free SiSb thin films (especially $Si_{(1-x)}Sb_x$, $x \sim 0.84$) has better thermal stability, less change in volume during phase change process, and low set/reset voltage and current compared with $Ge_2Sb_2Te_5$ thin films in nonvolatile phase change memory. However, some basic physical properties of SiSb, such as optical and dielectric properties in amorphous and crystalline state, remain unclear.

The initialization process is commonly required by a phase change memory in order to create uniform initial crystalline states. For a rewritable phase change optical disk, initialization has often been carried out by using a commercial initializer with continuous-wave (CW) laser scanning. For a phase change random memory, the phase change thin film is typically crystallized to a uniform initial state during heating in the CMOS process (i.e., passivating at 250–400 °C). Both initialization processes have been performed under near equilibrium conditions. In addition to studying the phase change dynamics under extra-non-equilibrium conditions (i.e., stimulated by pulsed laser or current) [12–14], determining the phase change characteristics of phase change memory thin films under near equilibrium conditions is also necessary. Studying these characteristics will be helpful in understanding the properties of both amorphous and crystalline states of materials, as well as in optimizing initialization parameters for phase change memories.

In this paper, the optical, dielectric and structural properties of $Si_{15}Sb_{85}$ phase change memory thin films under a moving CW laser irradiation with different power densities was investigated. Spectral ellipsometry and high-resolution transmission electron microscopy were employed. The corresponding initialization (i.e., crystallization of as-deposited thin films under near equilibrium thermal conditions) mechanism was analyzed and discussed.

2. Experimental

Sb-rich SiSb thin films with thickness of 76.5 nm were deposited on polycarbonate disc substrates at room temperature using DC magnetron sputtering. An antimony target with purity of 99.999% and diameter of 180 mm was used for co-

* Corresponding author.
E-mail address: ywang@siom.ac.cn (Y. Wang).

0925-8388/$ – see front matter © 2011 Elsevier B.V. All rights reserved.
doi:10.1016/j.jallcom.2011.02.031

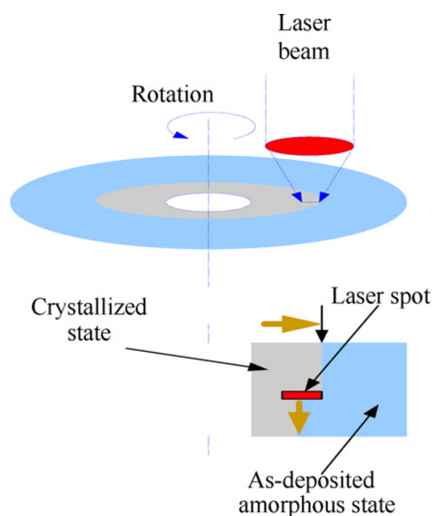

Fig. 1. Schematic principle of initialization using the POP120-5F phase-change optical disc initializer.

sputtering with some Si chips. The Si chips were placed symmetrically on the erosion area of the Sb target. The targets were bonded to water-cooled copper plates. Typically, the required base pressure in chambers is 6.4×10^{-4} Pa. In the experiment, sputtering was performed using Ar gas at a pressure of 0.6 Pa. The thickness of Sb-rich SiSb thin films were measured using an Alpha-step 500 (Tencor America Company) surface profiler. The composition of Sb-rich SiSb thin films were measured by energy dispersion spectra (EDS) equipped on SEM (JSM-6360LA). The composition of the Si and Sb component were about 15 at.% and 85 at.%, respectively. A POP120-5F phase-change optical disc initializer (Hitachi Computer Peripherals Co., Ltd.) was used to initialize the films at different CW laser powers. The wavelength of the laser was 810 nm and laser beam spot size was 1 μm × 192 μm (full width at half maximum, @1800 mW). Initialization was carried out at a constant linear velocity of 4 m/s. A Sopra GES5E UV/Vis/IR spectral ellipsometer (SE) was used to measure the ellipsometric parameters of films. The commercial software, WINELLI II, was applied to determine the best fit of optical and dielectric constants from measured ellipsometric parameters. Samples were immersed in chloroformic solution. Then, the salvaged fragments of thin films were fished out onto copper meshes with ultra-thin carbon film for TEM observation. High-resolution transmission electron microscopy (HRTEM) (JEOL-2010F) was utilized to analyze the structural characteristics of films.

3. Results and discussion

Fig. 1 illustrates the principle of laser initialization as exhibited. The as-deposited amorphous phase change thin films were crystallized to different extents and with adjustable initialization parameters (e.g., laser power and rotation speed).

The different initialized regions under different laser powers were distinguishable and could be marked easily by optical microscopy (Fig. 2).

The optical and dielectric properties of laser-initialized $Si_{15}Sb_{85}$ thin films at the ultraviolet (UV), visible, and infrared (IR) regions were characterized using a spectroscopic ellipsometer. Compared with traditional reflectivity measurements, the ratiometric nature of ellipsometry could determine the submonolayer sensitivity by detecting the polarization change of the reflected beam [15]. The complex refractive index ($N = n + ik$) and dielectric functions ($\varepsilon = \varepsilon_r + i\varepsilon_i$) of the thin films were calculated by fitting the measurable ellipsometric parameters, tan (Ψ) and cos (Δ), to a proper dispersion model.

The refractive indexes, extinction coefficients, and absorption coefficients of as-deposited and laser-initialized $Si_{15}Sb_{85}$ thin films at the wavelength range of 190–2300 nm (6.50–0.54 eV) are shown in Fig. 3. The absorption coefficients were calculated using the formula, $\alpha = 4\pi k/\lambda$, where α, k, and λ denote absorption coefficient, extinction coefficient, and wavelength, respectively.

As shown in Fig. 3(a), the refractive indexes of thin films increase gradually with wavelength from UV to visible region until they achieve the maximum at the IR region. This typical anomalous dispersion originates from the absorption band (Fig. 3(b)) according to the Kramers–Kronig relation [16].

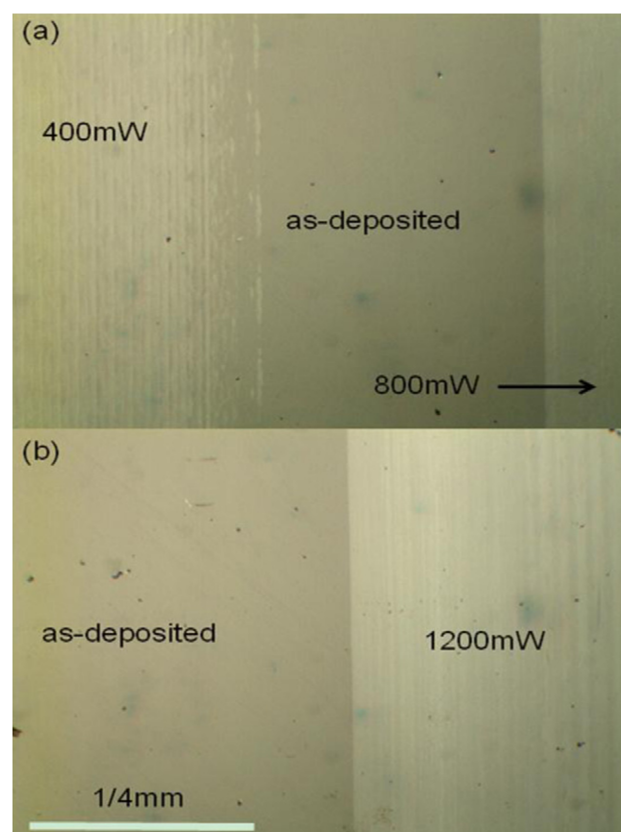

Fig. 2. Optical microscopic images of as-deposited and laser-initialized region on SiSb films.

The corresponding peak wavelength of refractive index and extinction coefficient shifted to the longer wavelength direction with increase in initialization power. The width of absorption band also became bigger as initialization power increased.

The intrinsic absorption band, as shown in the UV–visible region of Fig. 3(b) and (c), corresponds to the electron transition from valence band to conduction band after absorption of photons and generation of electron–hole pairs. After initialization with different laser powers, the change in the energy band structure was obvious. The optical band gaps of four different films were determined by fitting the absorption edges.

Absorption coefficient α and optical band gap E_g of the semiconductors generally follows a relationship in the form, $\alpha E = B(E - E_g)^n$ [17], where B is a parameter that depends on the transition probability, E is the energy of photon, E_g is the energy of the transition, and n is a number that characterizes the transition process. The plot of $(\alpha E)^{1/n}$ vs. E with $n = 2$ has very high linearity within a broad energy range at low photon energies and the values of optical band gaps can be linearly extrapolated, as shown in Fig. 4. The optical band gaps for the as-deposited film and initialized films at 400, 800, and 1200 mW are 0.42, 0.29, 0.23, and 0.20 eV, respectively. In some early works, by using $n = 2$, Tauc et al. [18] and Lee et al. [19] successfully fitted out the band gaps of GeTe and $Ge_2Sb_2Te_5$ films.

Near the intrinsic absorption edge, there is an absorption peak in longer wavelength range, as shown in the <1 eV region of Fig. 3(c), for as-deposited SiSb thin film, which might contribute to excitons absorption, a light absorption effect of electron-hole pairs in amorphous solid [20,21]. Incidentally, the influence of initializa-

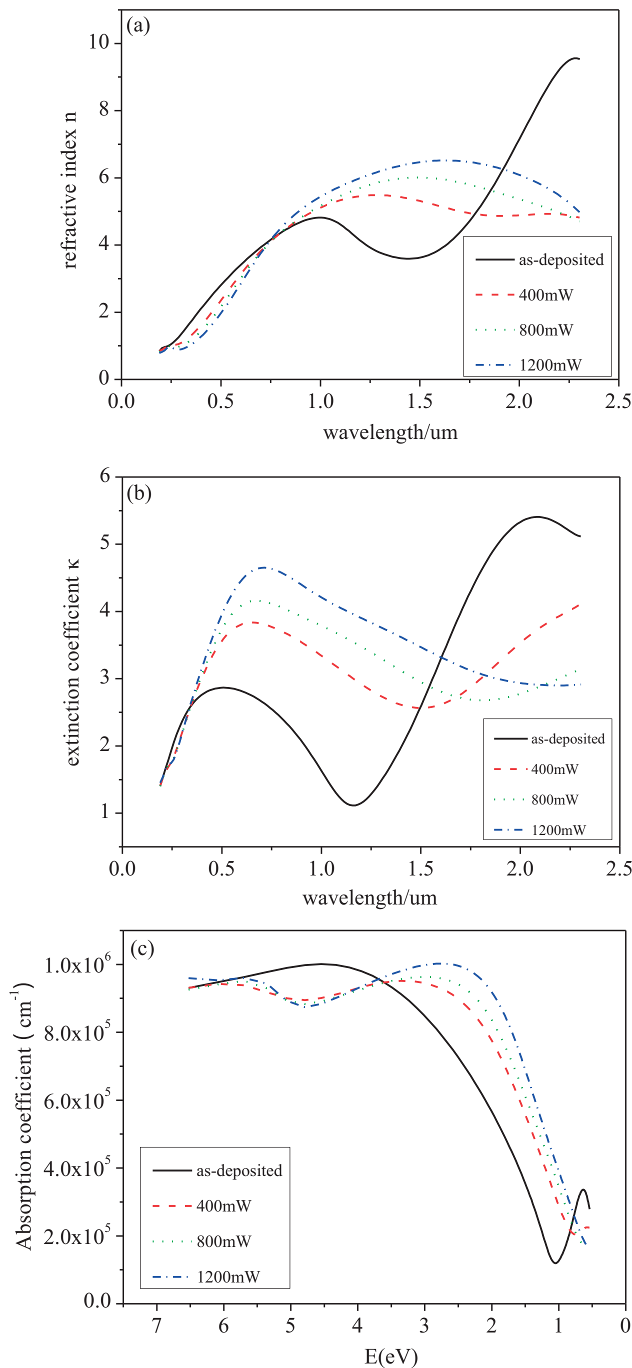

Fig. 3. Refractive indexes (a) of extinction coefficients (b) and absorption coefficients (c) for as-deposited and laser-initialized $Si_{15}Sb_{85}$ thin films at 400, 800, and 1200 mW.

tion power on exciton absorption could not be obtained due to the limitations in measuring wavelength ranges.

Dielectric properties are very important for resistive memory materials. Real part ε_r and imaginary part ε_i of the complex dielectric function are related to the n and k of the complex refractive index by the following equations: $\varepsilon_r = n^2 - k^2$ and $\varepsilon_i = 2nk$. The dependence of ε_r and ε_i on wavelength is shown in Fig. 5. Parameters ε_r and ε_i automatically obey the Kramers–Kronig relation. The variation of dielectric function with photon energy indicates that some interactions between photons and electrons in the films occur within this energy range [22,23]. Similar to optical constants, the real and imaginary parts of the complex dielectric function were

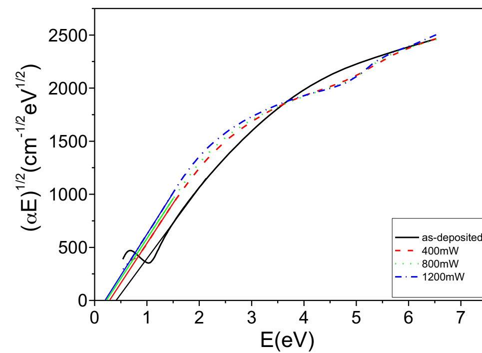

Fig. 4. Plots of $(\alpha E)^{1/2}$ vs. photon energy E for as-deposited and laser-initialized SiSb thin films.

related to storing and loss of energy within the medium in a specified wavelength (or energy) range. The position and amplitude of the dielectric function peak changed with initialization power. This energy dependence reflects the fact that the polarization of a normal material does not respond instantaneously to an applied field. The polarizability change might have been due to difference in chemical bonding [24]. Bonding can have a profound effect on local atomic arrangement. In relation, the local structures of as-deposited and laser-initialized films were analyzed in detail under high resolution.

The TEM and SAED (selective area electron diffraction) patterns of as-deposited and initialized SiSb films are shown in Fig. 6.

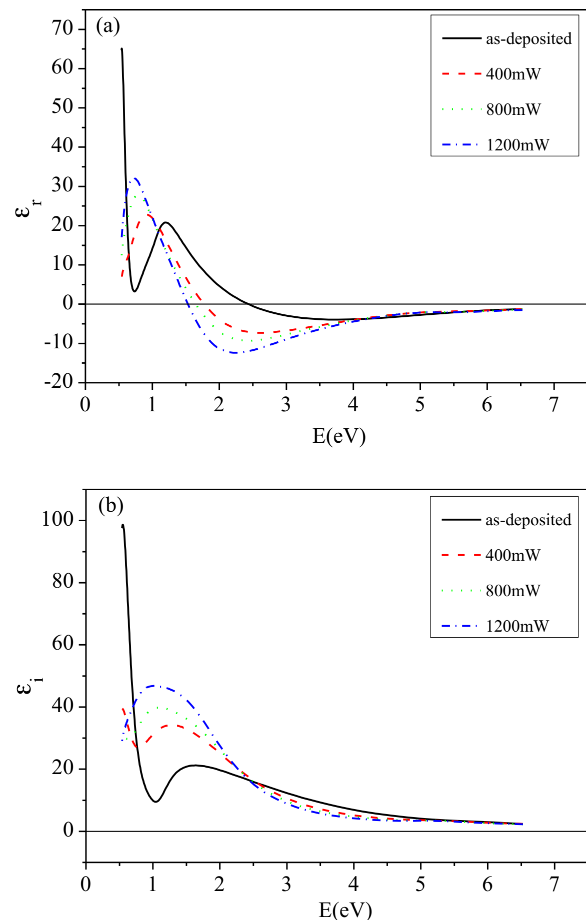

Fig. 5. Real (a) and imaginary (b) parts of the dielectric function of as-deposited $Si_{15}Sb_{85}$ film and $Si_{15}Sb_{85}$ films initialized by laser at 400, 800, and 1200 mW.

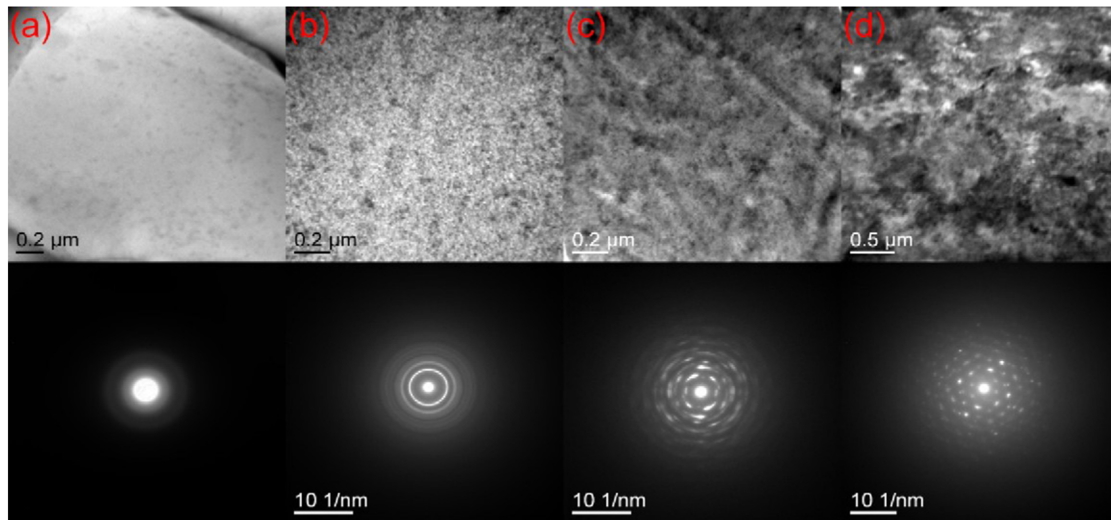

Fig. 6. TEM and SAED patterns of four kinds of films: (a)–(d) represent as-deposited film and films initialized by continuous laser at the power of 400, 800, and 1200 mW.

The as-deposited $Si_{15}Sb_{85}$ thin film was amorphous. With increments in initializing laser power, the crystallization extent of the films increased gradually and the grains became bigger. The crystalline phase corresponds to a distorted rhombohedra-Sb-like structure, as a small amount of Si atoms substitute for Sb atoms, causing the imperfection of rhombohedral Sb lattice [12].

In order to observe the arrangement of atoms, the different kinds of samples were thinned before HRTEM observation. Fig. 7 shows the HRTEM images and corresponding SAED patterns of as-deposited and laser-initialized SiSb thin films.

In Fig. 7(a), the as-deposited $Si_{15}Sb_{85}$ film is pure amorphous without any obvious crystallites. After initialization under low-power continuous laser (400 mW), the film was crystallized to an extent, after which polycrystalline phase formed with some concurrent amorphous phase regions (Fig. 7(b)). With incremental initialization in laser power, the crystalliza-

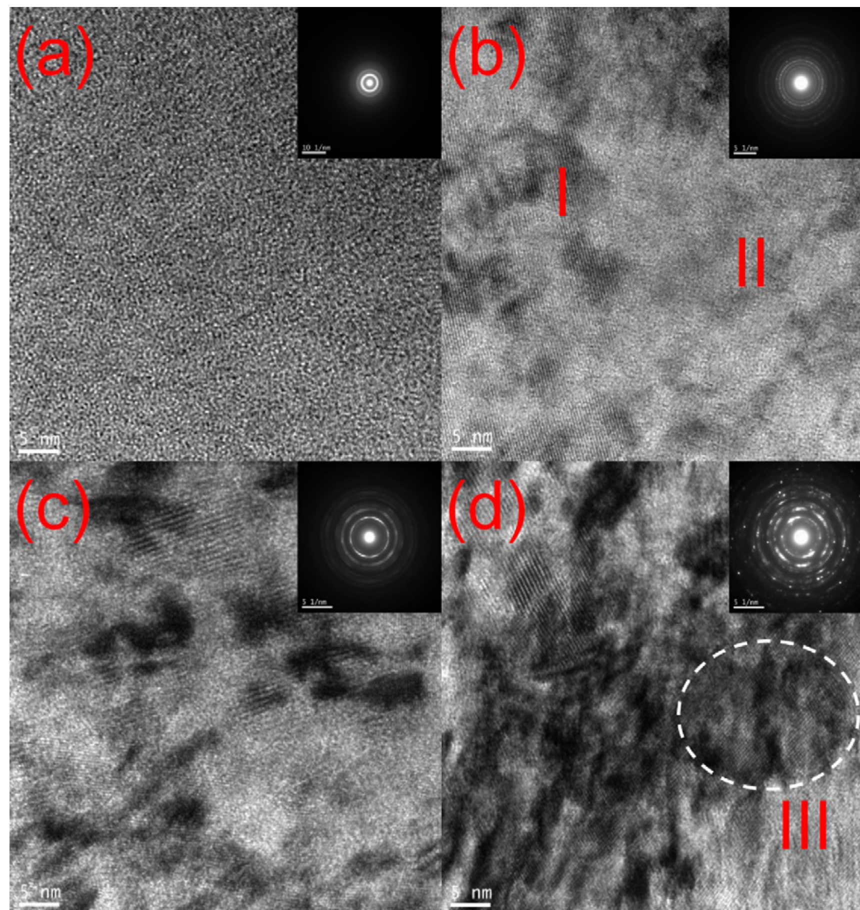

Fig. 7. HRTEM images and SAED patterns of as-deposited SiSb thin film (a) and films initialized by continuous laser at powers of 400 mW (b), 800 mW (c), and 1200 mW (d). Zone I represents the crystalline area; Zone II, the amorphous area; and Zone III, the rhombus-like structure area.

Table 1
Lattice parameters of crystalline Sb in PDF 35-0732 and lattice parameters calculated from SAED patterns of Fig. 6(b)–(d) for the corresponding crystallized samples.

Crystalline Sb in PDF35-0732			Crystalline Si15Sb85 at different initialization laser powers					
a = 4.307 Å		c = 11.27 Å	400 mW		800 mW		1200 mW	
d	h k l	Int-f	d	Error	d	Error	d	Error
3.753	0 0 3	25					3.801	±0.177
3.538	1 0 1	4						
3.109	0 1 2	100	3.08	±0.114	3.127	±0.117	3.127	±0.117
2.248	1 0 4	70	2.513	±0.075	2.296	±0.063	2.296	±0.063
2.152	1 1 0	56	2.145	±0.055	2.145	±0.055	2.145	±0.055
1.929	0 1 5	12			1.947	±0.045	1.947	±0.045
1.878	0 0 6	35	1.834	±0.04				
1.77	2 0 2	26			1.777	±0.037	1.777	±0.037
1.555	0 2 4	15	1.526	±0.027	1.563	±0.029	1.563	±0.029
1.479	1 0 7	13						
1.437	2 0 5	12			1.426	±0.024	1.426	±0.024
1.416	1 1 6	63	1.314	±0.02	1.366	±0.022	1.369	±0.022
1.252	0 0 9	25					1.257	±0.019
1.243	3 0 0	30						
1.219	0 2 7	11						
1.0768	2 2 0	12	1.117	±0.015			1.086	±0.014
1.0609	2 1 7	16						
1.0369	3 0 6	17						

tion extent of films increased and the amorphous phase region was reduced (Fig. 7(c) and (d)). The grain size of the polycrystalline phase increased with enhanced crystallization (see inset of SAED patterns in Fig. 6). When initialization laser power reached 1200 mW, crystalline grains exhibited a characteristic of single crystal (see SAED pattern in Fig. 6(d)). Meanwhile, a rhombus-like structure can be clearly observed from HRTEM image in Fig. 7(d).

According to the SAED patterns shown in Fig. 6 (b)–(d), we can also confirm that the polycrystalline grains in the film belong to the distorted rhombohedra-Sb-like structure. Table 1 enumerates the lattice parameters of laser-initialized SiSb films calculated from the SAED patterns. The parameters of crystalline Sb in powder diffraction file (PDF) 35-0732 are also listed for comparison.

4. Conclusions

The complex refractive index and complex dielectric function at the wavelength range of 190–2300 nm (6.50–0.54 eV) of as-deposited and CW laser-initialized $Si_{15}Sb_{85}$ phase change thin films have been obtained with the aid of spectroscopic ellipsometry. The corresponding peak wavelength has shifted to a longer wavelength (lower photon energy) direction with increase in initialization power. Both the width of optical absorption band and dielectric loss band increased with a rise in initialization power. These phenomena may contribute to changes in energy band structure after initialization. The optical band gaps of the as-deposited film and initialized films at 400, 800, and 1200 mW are determined by fitting the absorption edges to 0.42, 0.29, 0.23, and 0.20 eV, respectively. The structural origin of laser initialization has also been confirmed under high-resolution TEM observation. The structural change from as-deposited pure amorphous phase to distorted rhombohedra-Sb-like crystalline structure with the increase of initialization laser power is clearly observable in sub-nanometer resolution. The dependence of macroscopic physical properties, microscopic local atomic arrangements of films, and relation between them in relation to crystallization film extents formed by different initialization powers can be helpful in understanding the phase change mechanism and design the practical phase change memory devices.

Acknowledgements

This work was supported partially by the National Basic Research Program of China (grant no. 2007CB935402) and the National Natural Science Foundation of China (grant no. 50872139, 60644002).

References

[1] S.R. Ovshinsky, Phys. Rev. Lett. 21 (1968) 1450.
[2] D. Lencer, M. Salinga, B. Grabowski, T. Hickel, J. Neugebauer, M. Wuttig, Nat. Mater. 7 (2008) 972–977.
[3] G. Zhang, D. Gu, F. Gan, Z. Sun, J. Guo, Chin. Opt. Lett. 2 (2004) 555–558.
[4] T. Nonaka, G. Ohbayashia, Y. Toriumib, Y. Morib, H. Hashimotob, Thin Solid Films 370 (1999) 258–261.
[5] M.H.R. Lankhorst, J. Non-Cryst. Solids 297 (2001) 210–219.
[6] S. Gu, L. Hou, Q. Zhao, R. Huang, Chin. Opt. Lett. 1 (2003) 716–718.
[7] T. Zhang, Z. Song, Y. Gong, Y. Lin, C. Xu, Y. Chen, B. Liu, S. Feng, Appl. Phys. Lett. 92 (2008) 113503–113513.
[8] N. Nobukuni, M. Takashima, T. Ohno, M. Horie, J. Appl. Phys. 78 (1995) 6980–6988.
[9] T. Zhang, Z. Song, F. Wang, B. Liu, S. Feng, Appl. Phys. Lett. 91 (2007) 222102.
[10] T. Zhang, Z. Song, F. Wang, B. Liu, S. Feng, B. Chen, Jpn. J. Appl. Phys. 46 (2007) L602–L604.
[11] T. Zhang, Z. Song, B. Liu, S. Feng, Semicond. Sci. Technol. 23 (2008) 055010.
[12] H. Huang, F. Zuo, F. Zhai, Y. Wang, T. Lai, Y. Wu, F. Gan, J. Appl. Phys. 106 (2009) 063501–63505.
[13] H. Huang, F. Zuo, F. Zhai, Y. Wang, T. Lai, Y. Wu, F. Gan, J. Phys. D: Appl. Phys. 43 (2010) 175401.
[14] G. Bruns, P. Merkelbach, C. Schlockermann, M. Salinga, M. Wuttig, T.D. Happ, J.B. Philipp, M. Kund, Appl. Phys. Lett. 95 (2009) 043108–43113.
[15] T. Shima, J. Kim, J. Tominaga, N. Atoda, J. Vac. Sci. Technol. A 19 (2001) 826.
[16] C. Bertarelli, A. Bianco, F. D'amore, M.C. Gallazzi, G. Zerbi, Adv. Funct. Mater. 14 (2004) 357.
[17] J.I. Pankove, Optical Processes in Semiconductors, Prentice-Hall, Englewood Cliffs (NJ), 1971.
[18] J. Tauc, R. Grigorovici, A. Vancu, Phys. Status Solidi 15 (1966) 627.
[19] B.S. Lee, J.R. Abelson, S.G. Bishop, D.H. Kang, B.k. Cheong, K.B. Kim, J. Appl. Phys. 97 (2005) 093509–93518.
[20] K. Huang, R.Q. Han, Solid State Physics, Higher Education Press, Beijing, 1988, in Chinese.
[21] F. Messina, E. Vella, M. Cannas, R. Boscaino, Phys. Rev. Lett. 105 (2010) 116401.
[22] F.X. Huang, Y.Q. Wu, D.H. Gu, F.X. Gan, Thin Solid Films 483 (2005) 251.
[23] M.M. El-Nahass, Z. El-Gohary, H.S. Soliman, Opt. Laser Technol. 35 (2003) 523.
[24] K. Shportko, S. Kremers, M. Woda, D. Lencer, J. Robertson, M. Wuttig, Nat. Mater. 7 (2008) 653–658.